Porosity Characteristics of Ultra-low Dielectric Insulator Films Directly Patterned by Nanoimprint Lithography[*]

Hyun Wook Ro[a], Ronald L. Jones[a], Huagen Peng[b], Hae-Jeong Lee[a],
Eric K. Lin[a], Alamgir Karim[a], Do Y. Yoon[c], David W. Gidley[b], and Christopher L. Soles[a,†]

[a]NIST Polymers Division, 100 Bureau Drive, stop 8541, Gaithersburg, Maryland 20899, USA;
[b]Department of Physics, University of Michigan, Ann Arbor, Michigan 48109, USA;
[c]School of Chemistry, Seoul National University, Seoul 151-747, Korea

ABSTRACT

Direct patterning of low-dielectric constant (low-k) materials via nanoimprint lithography (NIL) has the potential to simplify fabrication processes and significantly reduce the manufacturing costs for semiconductor devices. We report direct imprinting of sub-100 nm features into a high modulus methylsilsesquioxane-based organosilicate glass (OSG) material. An excellent fidelity of the pattern transfer process is quantified with nm precision using critical dimension small angle X-ray scattering (CD-SAXS) and specular X-ray reflectivity (SXR). X-ray porosimetry (XRP) and positron annihilation lifetime spectroscopy (PALS) measurements indicate that imprinting increases the inherent microporosity of the methylsilsequioxane-based OSG material. When a porogen (pore generating material) is added, imprinting decreases the population of mesopores associated with the porogen while retaining the enhanced microporosity. The net effect is a decrease the pore interconnectivity. There is also evidence for a sealing effect that is interpreted as an imprint induced dense skin at the surface of the porous pattern.

Keywords: nanoimprint lithography, organosilicate, PMSQ, direct NIL patterning, PALS, X-ray reflectivity, XRP

1. INTRODUCTION

NIL is emerging as a next-generation patterning technique with enormous potential.[1-4] The allure of this technology is the inherent compatibility of a stamping process for high volume manufacturing combined with a patterning resolution comparable to electron beam lithography. There are many examples of features 10 nm and smaller fabricated via imprint technologies.[4-7] More recently, NIL has attracted attention for reasons other than resolution and throughput. It is also capable of replicating complex multi-level or 3-D patterns with a single imprint.[7-11] Conventional optical lithography requires multiple patterning steps through a layer-by-layer assembly process to fabricate multi-level structures. Furthermore, NIL has the potential to directly pattern a range of materials, not just sacrificial resists that are used with additive or subtractive processes to transfer the pattern into a functional material. The ability to directly pattern complicated structures into functional materials without etching or deposition has the potential to simplify fabrication and reduce manufacturing costs.

There is particular interest in directly patterning spin-on silsesquioxane materials,[12-14] especially for their use as interlayer dielectric (ILD) insulators in semiconductor devices.[10,11] State-of-the-art microprocessors require eight or more layers of wiring in the interconnect infrastructure to pass the electrical signal into and out of the transistors. The current optical lithography patterning combined with dual damascene methods require approximately 20 processing steps for each layer of wiring and it has been suggested that imprinting the interconnect material with a two-tier mold that produces a T-gate structure in a single imprint has the potential to cut the number of lithography steps in half.[11] Directly patterning the dielectric insulator would also eliminate several pattern transfer (etching and deposition) steps, greatly simplifying device fabrication.

ILD materials today, which are used in their fully dense form, have dielectric constants on the order of $k \sim 2.9$. For next generation devices, k needs to be reduced significantly to minimize the cross-talk and capacitive coupling between the adjacent interconnect lines, decrease power consumption, and decrease the capacitive delay of the circuitry. This can only be realized by introducing large amounts of nanoscale porosity into the ILD material.[15-17] The imprint literature on this topic thus far has been limited to demonstrating the feasibility of directly patterning non-porous ILD materials from the pattern transfer point of view.[10,11] Here we make the crucial jump to imprinting *porous* ILD materials. However, the porous versions of these materials are mechanically fragile in most cases and this has precluded porous ILDs from being implemented into current semiconductor devices; the harsh integration processes often induce mechanical failure or fracture.[18-21] There are natural concerns of whether these mechanical liabilities will be exacerbated by direct nanoimprinting, given that the patterns will be created through a mechanical deformation of the material. There is also the possibility, however, that eliminating some of the harsh etching and polishing integration procedures that lead to ILD failure mitigates some of these problems.

Equally as important as imprinting and inducing porosity is to quantify how the imprint process impacts the characteristics of the porosity. Small, isolated pores that are not interconnected are highly desirable because they minimize the potential for Cu ion migration between interconnect lines, reduce the potential for resist poisoning of the dielectric, and generally perform as better barrier materials.[15-17] To perceive subtle changes in the pore structure of such nanoporous ILDs, especially in their patterned form, is a metrology challenge. To address this challenge we develop and apply XRP [22,23] and positron annihilation spectroscopy [24-26] to quantify the porosity characteristics in these porous patterns. This is combined with quantitative, high-resolution measurements of the pattern shape using SXR [27,28] and CD-SAXS [29,30] to develop a comprehensive understanding of how direct imprinting impacts these ILD materials.

2. EXPERIMENTAL

Direct patterning of Poly(methylsilsesquioxane)s (PMSQ)s: The PMSQ-based prepolymer film and film with 20 vol-% of porogen (Tetronic[§], T150R1) were spin cast at 209 rad/s (2000 rpm) onto 10.16 cm diameter Si wafer with a native oxide. The imprints were made under vacuum in two steps: 10 s at 100 °C and 1.4 MPa followed by 3 min at 200 °C and 3.4 MPa. The tool was cooled to 55 °C before releasing the pressure. The pattern was separated from the mold at room temperature. The imprints both with and without porogen were vitrified at 430 °C in a nitrogen environment.

Specular X-ray reflectivity (SXR) & X-ray porosimetry (XRP): SXR measurements were performed on a Philips model X'PERT MRD reflectometer using a finely focused copper $K\alpha$ radiation (λ=1.54 Å) source. The reflectivity was collected at room temperature to determine the critical angle of the sample in a vacuum. Next, the sample chamber was saturated with toluene vapor at 25 °C for 1 hour after which the reflectivity was measured again.

Positronium annihilation lifetime spectroscopy (PALS): PALS measurements were performed in the vacuum chamber of an electrostatically-focused positron beam with ^{22}Na as the radioactive source of positrons. Four positron beam energies, namely (0.55, 1.2, 2.2, and 2.7) keV, were utilized to control the implantation of positrons into the films. The corresponding mean implantation depths are (10, 38, 100, and 150) nm respectively for the film with density of 1.0 g/cm^3. The lifetime spectra were fitted using both discrete and continuum fitting programs, i.e., POSFIT and CONTIN, to resolve positron/positronium lifetimes and intensities and pore size distribution (PSD).

3. RESULTS AND DISCUSSION

Previously we reported a terpolymer silsesquioxane (a copolymer of methyltrimethoxysilane, 1,2-bis(triethoxysilyl)ethane, and dimethyldimethoxysilane) resin, which is optimized to meet many of the required properties for an ILD material, including a $k = 2.84 \pm 0.05$ measured at 1 MHz, a Young's modulus of (10.5 ± 0.5) GPa, and a coefficient of thermal expansion of $(19.2 \pm 1.7) \times 10^{-6}$ °C^{-1}.[31,32] We suspect that the relatively high modulus of this material will be an important factor for retaining the structural integrity of a porous imprinted feature. This material is

---

[§] Certain commercial materials and equipment are identified in this paper in order to specify adequately the experimental procedure. In no case does such identification imply recommendation by the National Institute of Standards and Technology nor does it imply that the material or equipment identified is necessarily the best available for this purpose.

readily made porous by adding a poly(ethyleneoxide)-*block*-poly(propyleneoxide) (PEO-*b*-PPO) surfactant (Tetronics, T150R1) as the porogen. The porogen volatilizes when the silsesquioxane is vitrified into a 3-dimensional glassy network at 430 °C, leaving pores in its place. Here we imprint both a non-porous and a porous version of this terpolymer. The porous sample is loaded with 20 % by volume of the porogen to yield, according to our previous experimental observations and the theoretical predictions, an ultralow dielectric constant of $k = 2.2$.[31,32]

SXR can quantify, with sub-nm precision, the pattern height, the residual layer thickness and the line-to-space ratio of parallel line-space gratings patterns, like those imprinted here.[27,28] Fig. 1(a) shows the SXR data in terms of log of the ratio R of the reflected to incident intensities as a function of the wave vector Q ($Q = 4\pi\sin(\theta)/\lambda$, where λ is the wavelength and θ is the angle of both incidence and reflection) for the imprinted films both with and without the porogen. Both of the curves in Fig. 1(a) correspond to the as-imprinted patterns before vitrification. In reflectivity there is a critical wave vector Q_c for each material, the square of which is proportional to the electron and thus mass density. Below Q_c all of the X-rays are externally reflected from a smooth surface of the material; above Q_c the X-rays penetrate into the material. In Fig. 1(a) a series of three pronounced reductions in the reflected intensity are observed, suggesting three Q_cs for three layers of different density in the sample. As described elsewhere in detail, [27,28] these three layers in order of increasing Q_c (increasing density) correspond to the region of the patterned dielectric material, a residual layer of unpatterned dielectric material beneath the patterns, and the supporting Si wafer substrate.
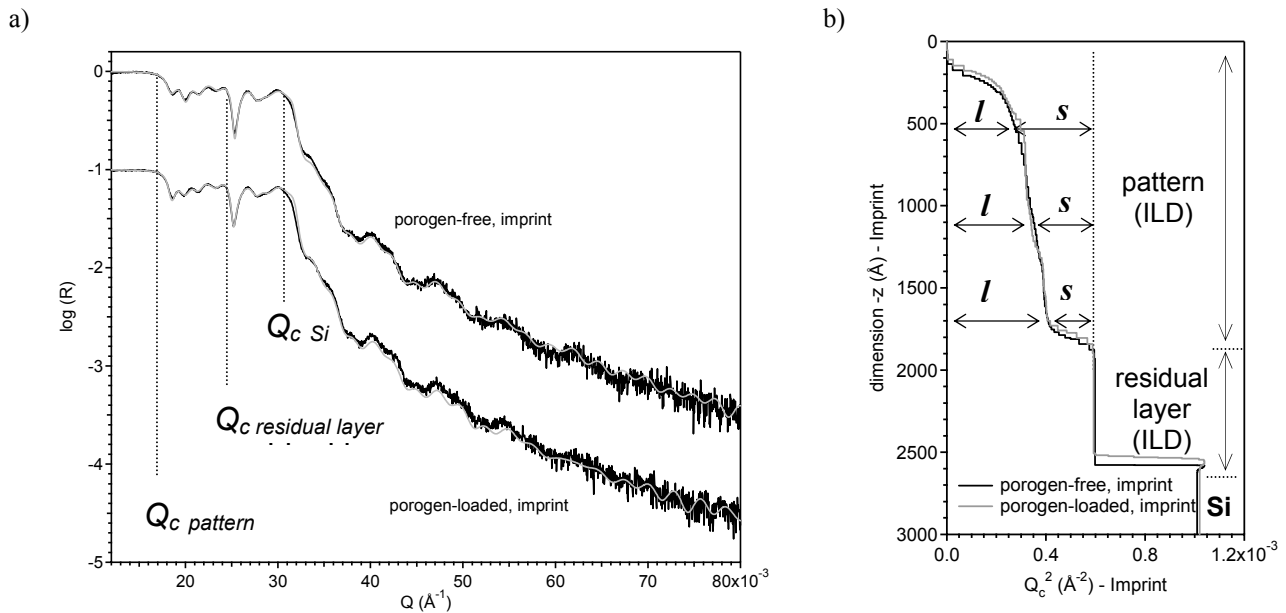

Fig 1. The reflectivity data and scattering length density profiles are shown for the different stages of the patterning process. Part (a) shows the raw reflectivity data (black) for the as-imprinted patterns of both the porogen-free and porogen loaded samples. Part (b) shows the scattering length density profiles corresponding to the fits in Part (a). A series of horizontal lines labeled "*l*" and "*s*" are superimposed on the profile to indicate the relative magnitude of the line and space widths a few different heights in the pattern region.

The three Q_cs are observed for two materials (ILD material plus Si substrate) because the coherence length of the X-ray source that SXR averages density over is larger than the pattern periodicity. The result is an effective density for the patterned region that appears less than fully dense dielectric material, reduced by a factor precisely equal to the line-width to pattern-pitch ratio. By fitting the reflectivity profile with a multi-layer recursive algorithm based on the formalism of Parratt,[33,34] it is possible to extract the density profile as a function of distance through the patterned region, the residual layer, and the supporting substrate. Fig. 1(b) shows the density depth profiles from the fits to the imprint reflectivity data in part (a). Here the density is represented on the horizontal axis in units of Q_c^2 (directly proportional to mass density) while the distance z is displayed on the vertical axis.

The annotations to Fig. 1(b) help orient the density profile with the physical features of the pattern. The total height for the imprint made into the porogen-free terpolymer is (1603 ± 10) Å[‡] with residual layer thickness of (766 ± 10) Å. For the patterns in the porogen-loaded terpolymer the pattern height and residual layer thickness are (1600 ± 10) Å and (757 ± 10) Å, respectively. To within error the imprinting process appears to be very reproducible; with or without porogen the same profile is obtained. Notice how the density profile in the region of the pattern height is not a vertical line. The effective density is greater near the residual layer interface and decreases towards the top of the patterns. This indicates that the pattern widths are tapered, slightly greater near their base. By comparing the Q_c^2 value in the patterned region to the Q_c^2 values of the fully dense dielectric material in the residual layer ($Q_c^2 = 6.0 \times 10^{-2}$ Å^{-2}) and the air gap between the patterns ($Q_c^2 = 0$ Å^{-2}), one can calculate the average line-to-space ratio as a function of pattern height as shown in Fig.1(b).
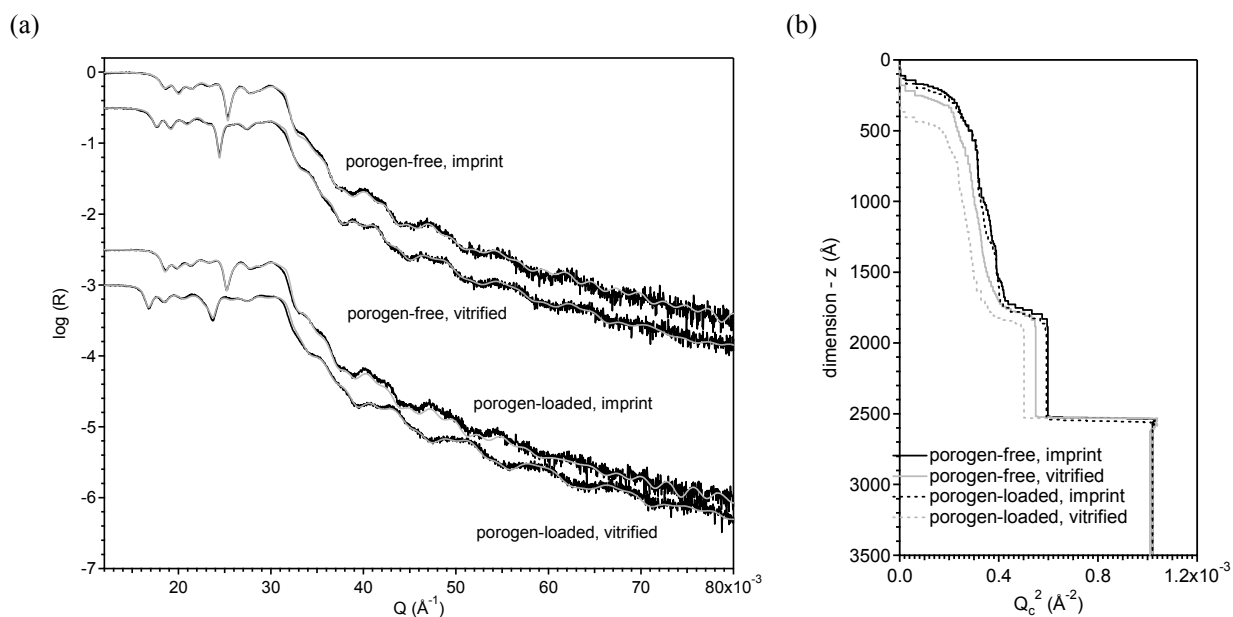
(a) (b)

Fig. 2. (a) The reflectivity data and (b) scattering length density profiles for before and after vitrification process for the porogen-loaded and porogen-free imprints.

Next the imprinted patterns are fully vitrified into a hard silicate. Fig. 2(a) shows the SXR data both before and after vitrification at 430 °C for the porogen-free and porogen-loaded patterns. Once again a series of three Q_cs corresponding to the patterned ILD material, the residual layer of unpatterned ILD material, and the supporting Si substrates are observed. Notice that the Q_c of the Si substrate does not change with vitrification, as to be expected. However the Q_cs of the patterned and residual layer shift to lower Q upon vitrification. This is more pronounced in the porogen-loaded sample owing to the generation of large quantities of mesoscale porosity; the density is significantly reduced. The slight shift to lower Q for the porogen-free sample reflects the creation of a small amount of microporosity in the dielectric material. This will be discussed later in detail.

Fig. 2(b) displays the density depth profiles from the fits to the experimental reflectivity data in part (c). Consistent with Fig. 1(b) the density profiles for the as-imprinted porogen-free and porogen-loaded samples overlap. However, after vitrification one finds that pattern heights shrink by approximately 4.0 % and 12.0 % in the porogen-free and porogen-loaded samples, respectively. This pattern height shrinkage is in contrast with a smaller decrease in the residual layer thickness of approximately 3.0 % and 9.0 % in the porogen-free and porogen-loaded samples, respectively. For some

---

[‡] The error bars presented throughout this manuscript indicate the relative standard uncertainty of the measurement.

reason greater vertical shrinkage occurs in the pattern region. As discussed later, we believe that this enhanced shrinkage in the pattern reflects an imprint-induced collapse of some of the mesoscale porosity. One also notices an overall reduction of the apparent density (uniform shift to smaller Q_c^2 values) throughout both the patterned region and the residual layer after vitrification; the porogen-free and porogen-loaded profiles no longer overlap. There are two possible explanations for this observation. One would be the generation of porosity without lateral shrinkage, where the line-to-space ratio stays the same. The second would be a lateral shrinkage where the line width decreases and the space width increases. SXR measurements alone are unable to distinguish between these two scenarios because, as discussed previously,[27,28] the in-plane directions are relative in terms of a line-to-space ratio; only the vertical or height dimension are absolute.

To resolve the uncertainties in the pattern widths and densities, CD-SAXS is used to absolutely measure the pattern widths. CD-SAXS is a transmission scattering technique capable of quantifying the full pattern cross-section (pattern shape).[29,30] The technique treats a periodic array of the patterns, such as those studied here, as a diffraction grating. By analyzing the diffraction patterns as a function of rotation angle it is possible extract the pattern shape and periodicity. For both the mold and the imprint patterns studies here, it turns out that a trapezoidal cross-section does an excellent job at approximating the experimental data. While we do not show the details of the analysis here (see References 29 and 30), Table I summarizes the average values of the width W, pitch Γ, height H, and sidewall angle β of the trapezoid model that best fits the CD-SAXS data for the mold, the as-imprinted, and the vitrified patterns. Notice that there is no change in Γ and almost no change in W for either the porogen-free or porogen-loaded patterns after vitrification, especially to within the level needed to explain the observed changes in Q_c^2. These findings suggest that the changes in Q_c^2 in the pattern density profiles of Fig. 2(b) after vitrification are affected by a change in the porosity or density, not lateral pattern shrinkage. It is noteworthy that vitrification induces a moderate shrinkage in the pattern height, but not pattern width.

Table 1. Average values of the width W, pitch Γ, height H, and sidewall angle β of the trapezoid model that best fit the CD-SAXS data for the mold, the as-imprinted, and the vitrified patterns.

	W (Å)	Γ (Å)	H (Å)	β (°)
imprint mold		1970 ± 10		
imprinted, porogen-free	1130 ± 10	1970 ± 10	1380 ± 100	7.1 ± 1.0
vitrified, porogen-free	1160 ± 10	1970 ± 10	1190 ± 100	5.1 ± 1.0
imprinted, porogen-loaded	1080 ± 10	1970 ± 10	1380 ± 100	6.1 ± 1.0
vitrified, porogen-loaded	1030 ± 10	1970 ± 10	1210 ± 100	7.0 ± 1.0

With the absolute measurement of the pattern width/pitch from the CD-SAXS, it is possible to convert the density profiles in the patterned region of Fig.1(b) and Fig. 2(b) into absolute pattern width variations as a function of the pattern height, i.e., define the pattern cross-section.[28] Fig. 3 shows the full pattern cross sections for all the samples. We see noticeable pattern shrinkage of the porogen-free and the porogen-loaded samples, respectively, in both the vertical and lateral directions relative to original dimensions of the mold. However, as shown in Fig. 1(b), the degree of shrinkage after imprinting was independent of whether the sample contained porogen or not. A small amount of shrinkage after imprinting is reasonable. After spin casting from solution, the films will retain a small fraction of the casting solvent. Imprinting at 200 °C under a vacuum will remove this residual solvent and induce shrinkage. The role of this residual solvent will be discussed later.
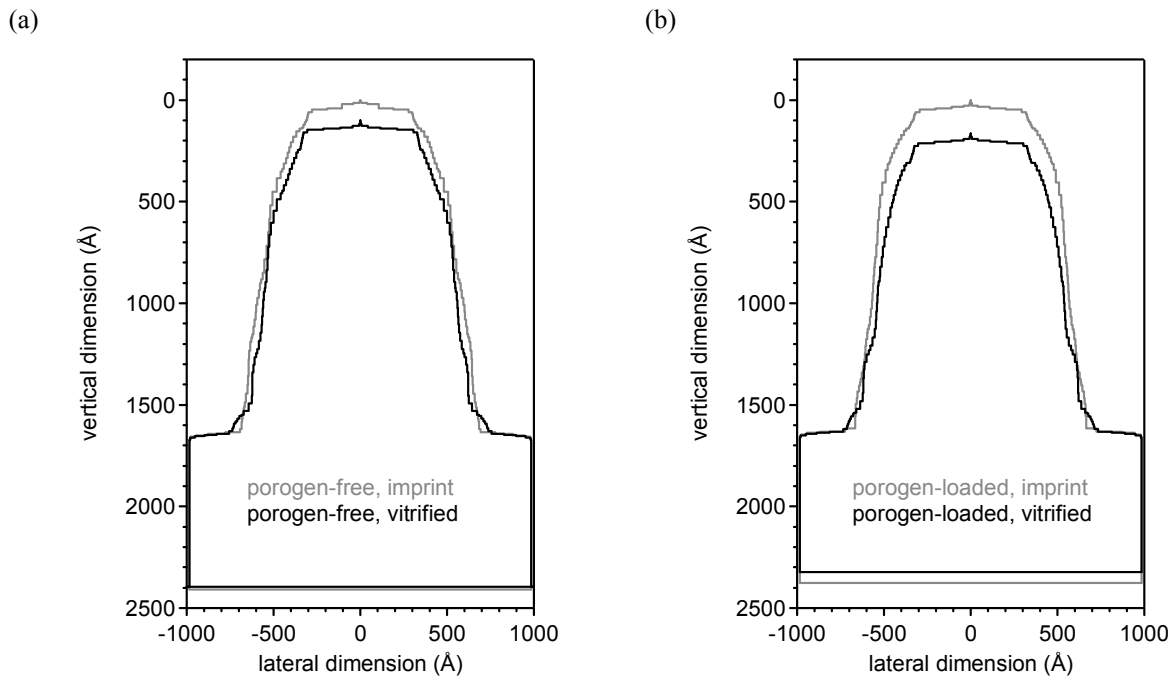
(a)

(b)

Fig. 3. By combining the scattering length density profiles in Fig. 1(b) and 2(b) with the CD-SAXS data presented in Table I, it is possible to quantify the average pattern cross-section of the imprinted patterns. This reveals shrinkage of the pattern from the original mold dimension in both the lateral and vertical directions. In parts (a) and (b) we see the pattern shape change upon vitrification for the patterns with and without porogen.

Fig. 3(a) and (b) show the vitrification effect on the pattern shape for the porogen-free and porogen-loaded patterns, respectively. In the case of the pattern without porogen, there is a small amount of vertical shrinkage of the pattern with almost no change in the pattern width. Vitrification has a minimal effect on the pattern fidelity. A slightly larger degree of vertical shrinkage is encountered in the pattern containing porogen, however, there is once again very little lateral shrinkage upon vitrification. That the patterns retain their shape with such high fidelity through the high temperature anneal is necessary for the direct pattering of ultralow-k dielectric materials.

Fig. 2(b) shows that the scattering length density profile of the patterns decreases during the vitrification process. The discussion of the CD-SAXS data and the pattern profiles in Fig. 3 indicates there is minimal change in pattern shape during vitrification, implying that the porosity or density of the material within the pattern must be changing. The porosity in the imprinted patterns after vitrification is quantified with XRP.[22,23] XRP combines SXR measurements with the condensation of an organic vapor inside the pores to characterize porosity. We find that toluene is an excellent probe vapor for silsequioxanes because it easily permeates through the matrix or wall material without swelling the cross-linked network. As toluene works it way through the material, it condenses in the small pores due to their small radius and capillary condensation. Replacing the air or vacuum inside the pores with toluene results in an appreciable change of the electron density of the material that can be quantified by SXR.

Fig. 4(a) shows the SXR data for the vitrified samples both under vacuum and in the presence of saturated toluene vapor. In each case the Q_c for the Si does not change in the presence of toluene but the Q_cs for the residual layer and patterned region of the dielectric insulator shift to higher Q; the condensation of toluene makes the ILD material denser. The increase in density is more pronounced for the porogen-loaded sample, consistent with the induced porosity. However, even the porogen-free sample adsorbs some toluene, indicating a small amount of intrinsic porosity. Fits to the SXR data in Fig. 4(a) are presented in Fig. 4(b) in terms of the scattering length density profiles for the porogen-free and porogen-loaded samples, revealing how the density of the pattern and residual layer increase with the absorption of toluene. The Q_c^2 increase is uniform as a function distance through the residual layer in both samples. From this data we determine

the porosity in the residual layer to be (11.4 ± 1.0) % and (21.5 ± 1.0) % for the porogen-free and porogen-loaded samples, respectively. Non-patterned versions of these films those were vitrified under identical conditions lead to porosities of (8.5 ± 1.0) % and (22.9 ± 1.0) %, respectively; the residual layer of the patterned, porogen-free material has slightly more microporosity than the unpatterned analog while they are within error for the porogen-loaded sample. The origins of this enhanced microporosity in the porogen-free residual layer will be discussed later.
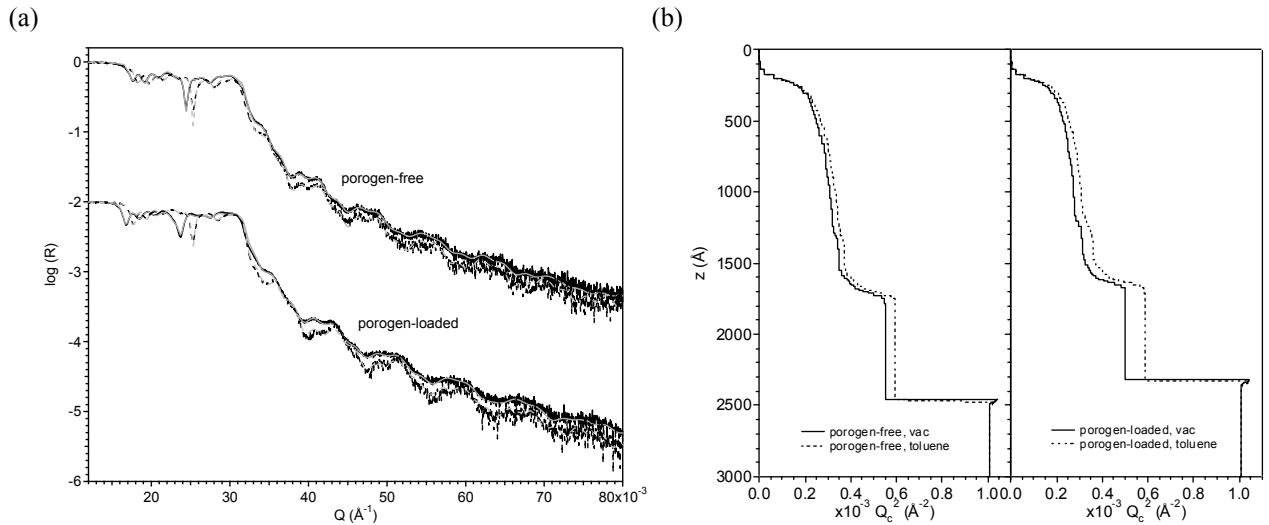
(a) (b)

Fig. 4. (a) Reflectivity data of the porogen-free and porogen loaded samples after vitrification both in vacuum (solid data) and in the presence of saturated toluene vapor (dotted data). Part (b) shows how the scattering length density profiles change upon the adsorption of toluene into the pores.

There is also an increase in Q_c^2 in the patterned region upon the adsorption of toluene. The absolute magnitude of this shift in Q_c^2 decreases with increasing height, and approaches zero at the top of the patterns. Fig. 3 already reveals that the pattern widths decrease with height, so a decrease in the absolute uptake with pattern height is expected. Thinner line widths mean less material and less adsorbed toluene on an absolute scale. However, since the absolute line widths are known, it is possible to renormalize the toluene adsorption data and properly account for the level of porosity within the patterned material as a function of pattern height. This renormalization is shown in Fig. 5 for both the porogen-free and porogen-loaded patterns. The horizontal dotted lines indicate the level of porosity in the residual layer. In the case of the porogen-free sample, the porosities in the patterned and unpatterned regions (residual layer) are very similar. However, in the porogen-loaded sample there is a significant decrease in the porosity with increasing pattern height, approaching the level of porosity in the porogen-free material at the top of the pattern; the porosity decreases with pattern height. The origin for this decreased porosity near the tops of the pattern is not yet obvious. Two possible explanations immediately come to mind. First, the induced porosity may arise from a second phase porogen. If the porogen were to be excluded during the imprint process, leaving just matrix material at the tops of the patterns, the observed porosity variations could be rationalized. However, it is also possible that the porogen remains well dispersed throughout the pattern and residual layer during the imprint process, and that upon vitrification the pores near the top and edges of the pattern preferentially collapse. Such a mechanism could also explain both the densification at the pattern tops as well as the enhanced vertical shrinkage upon vitrification relative to the porogen-free sample. However, we are unable to distinguish between the two mechanisms and in all likelihood the proper explanation may be a combination of the two effects.
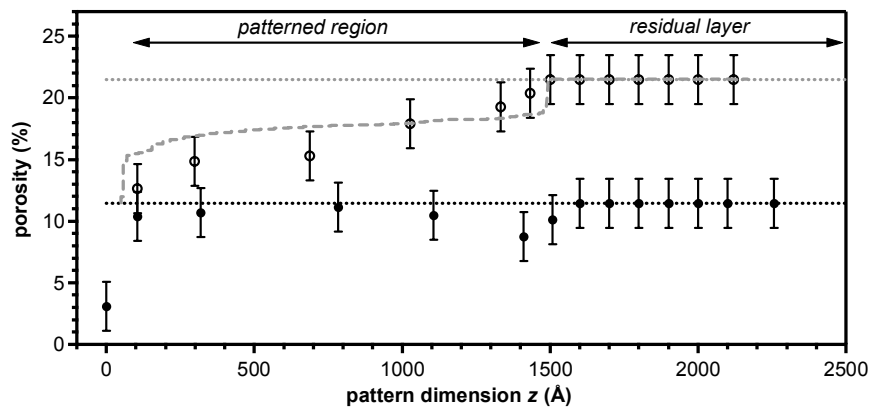
Fig. 5. The porosity with respect to the pattern height are plotted for the porogen-loaded sample (grey data) and the porogen-free sample (black data).

Depth-profiled PALS measurements provide deeper insight as to how imprinting affects the pores of these materials. PALS is a pore/void volume characterization technique performed in a vacuum whereby the shortening of the annihilation lifetime of positronium (Ps) due to collisions with the pore walls is directly correlated with the pore size. [24,25] In addition, the signal of Ps that escape from the film and annihilate in vacuum is used to quantify the pore interconnectivity. [26] Fig. 6(a) shows the PALS-deduced pore size distributions (PSD) for vitrified samples of the porogen-free and porogen-loaded samples both with and without patterning. The patterned samples are exactly the same as those employed for the XRP measurements displayed in Fig. 4 and 5. The unpatterned samples studied by PALS correspond to separate planar films that have been directly vitrified without going through the imprint process. The porogen-free films in black have PSD typical of a silsesquioxane matrix: a bimodal distribution of closed (not interconnected) micropores with average pore diameters (assumed spherical) of approximately 0.5 nm and 1.1 nm. The act of patterning this material appears to shift both peaks of this bimodal distribution to pore diameters that average (10 to 12) % larger, consistent with an increase in the microporosity. This increase in microporosity is quantitatively consistent, to a first approximation, with the XRP report of an increased porosity of 11.5 % by volume in Fig. 5 versus the nominal 8.5 % by volume porosity for unpatterned versions of this film. Hence, imprinting appears to enlarge native micropores of the matrix material. We suspect that this may reflect residual solvent being trapped during the imprint and acting as a molecular scale porogen. Once the mold is pressed into the film it will be difficult for residual solvent to escape the system.

The porogen-induced pores are observed in Fig. 6(a) as an additional population above 1.5 nm, as a peak in the PSD in the (2.0 to 2.2) nm range. Comparing the PSDs of the two unpatterned films (solid curves), we estimate that these larger pores account for approximately about 2/3 of the film porosity, consistent with XRP-deduced porosities of 8.5 % and 22.9 % respectively. The more interesting observation is the effect of imprinting on the porogen-loaded sample. Fig. 6(a) shows a significant decrease in the population of large pores and an increase in the population of micropores relative to the unpatterned material. From the applications point of view, this is an extremely attractive and unexpected result of the imprint process. It is generally realized that small pores are superior for ultralow-k materials because they have the potential to minimize, depending on their spatial distribution, percolation or interconnection problems. The fact that imprinting decreases the mesopore population and increases the micropores is a very attractive step in reaching this goal. This being said the shift in the PSD probably coincides with a decrease in porosity and hence an increase in the effective k for the film.

PALS is also well-suited for detecting pore interconnectivity through the fraction of Ps that diffuses through the interconnections and escapes back into vacuum. [26] When the total film porosity approaches 23 % by volume, it is reasonable to see signs of interconnections in the PALS response. Fig. 6(b) shows the Ps escape fraction for a few different Ps implantation depths (the deepest of which extend into the Si substrate) for the vitrified samples containing

porogen both with and without patterning. There is a statistically significant reduction in the Ps escape fraction for the imprinted pattern, which is entirely consistent with the reduction of the population of larger pores in Fig. 6(a). This is also consistent with greater vertical shrinkage in the patterned porous film seen in Figure 3(b), suggesting that a pore collapse mechanism leading to shrinkage may be appropriate.

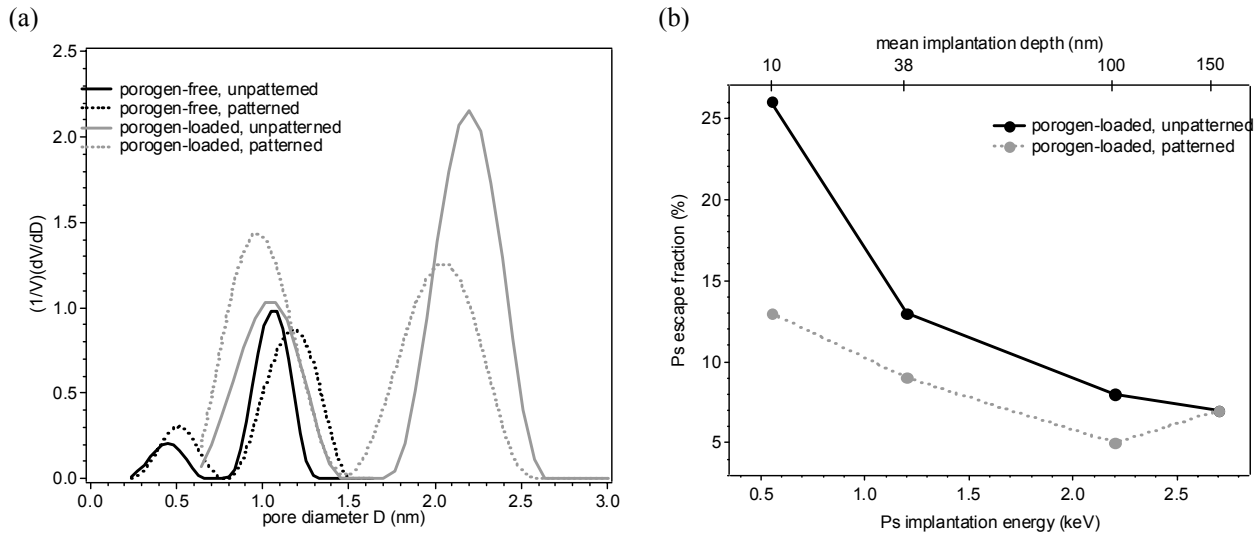(a)   (b)

Fig. 6. The pore size distributions of the four dielectric films fitted from the PALS spectra acquired at 2.7 keV using the CONTIN program are shown in part (a). The area under the PSD curve scales with the XRP measured porosity of the entire film for unpatterned films and the residual layer for the patterned film. The Ps escape fraction, i.e., the relative amount of escaping vacuum Ps vs. the combined Ps intensity owing to porogen-induced pores, is plotted against positron implantation energy in part (b). The Ps escape fraction typically increases with the decreases in beam energy, as Ps formed from shallowly implanted positrons are more prone to escape.

The combination of a vertical shrinkage upon vitrification, the reduced population of the porogen-induced pores, the strongly attenuated Ps escape fraction, and a porosity at the top of the pattern that is consistent with the porogen-free material would be consistent with a dense skin of non-porous material at the surface of the pattern. Fig. 2(b) shows a collapse in pattern height of approximately 200 Å upon vitrification. As a crude approximation, assume that the pattern with the porogen-induced porosity has a uniform 200 Å thick skin of higher density material surrounding the pattern and that this skin has the same density as the residual layer of the porogen-free materials (11.5 % porosity). Also assume that the center of this pattern has the same 21.5 % porosity as the residual layer for the porogen-loaded sample. Since the pattern is tapered, the dense skin is a greater fraction of the total porosity towards the top of the pattern, giving rise to a decrease in porosity with pattern height. Since the width of the pattern is known as a function of pattern height, it is possible to calculate the porosity as a function of pattern height for the simplified model. The grey dashed line in Fig. 5 indicates that the simple dense skin model does a reasonably good job of describing the porosity variations as a function of height. All of the data presented here seem consistent with the notion that imprinting induces a dense skin on the pattern for the porogen-containing materials.

One could conceive several different mechanisms by which a dense skin would arise at the surface of the porogen-loaded imprints. Previously we have alluded to a pore collapse mechanism. This would be reasonable at an interface where stresses only biaxial stresses can exist; an inability to support a triaxial stress near an interface may be relevant to pore collapse. However, it is unclear whether these continuum mechanics arguments are valid for 2 nm pores near an interface. It should also be realized that the moderately hydrophilic PEO domains of the porogen are not compatible with the very hydrophobic nature of the fluorinated mold surface. During the imprint process there would be an energetic driving force for a porogen-depleted region to develop near the mold interface. In reality, the situation is probably even more complex. In addition there will be large amounts of shearing during the imprint as the material slides past the static surfaces of the mold and into the cavities. These shear fields could alter the shape of the porogen domains and

possibly even their phase behavior with the matrix material in a very non-trivial manner. At this time the exact nature of the dense skin is still unclear. We suspect that the mechanism is pore collapse, but this remains to be verified.

4. CONCLUSION

These initial measurements indicate that imprint processes have great potential for directly patterning the dielectric insulator materials used in semiconductor fabrication. Patterns can be both imprinted and vitrified while retaining a high degree of fidelity with respect to the shape and size of the features in the imprint mold. These patterns can also be made porous through the use of a second phase porogen. However, there appears to be a moderate reduction of the mesoscale porosity generated by the porogen (consistent with observed film shrinkage) in the region of the pattern. One effect of this reduced mesoscale porosity will be to increase the effective k of imprinted pattern. Perhaps more importantly, the reduced porosity seems to be selectively isolated to the surface of the pattern, effectively forming a dense skin. This may turn out to be beneficial given that in conventional lithography extra processes are implemented to construct barriers on the surface of ILD patterns to reduce interdiffusion.[35-37] Direct imprinting may have the potential to naturally enhance the barrier properties of the ILD pattern. It is also beneficial that the imprinted reduced mesoscale porosity is partially off-set by an increase in the microporosity native to the ILD material. Isolated micropores are generally superior to mesopores for barrier properties.

5. ACKNOWLEDGEMENTS

6. REFERENCES

[1]   Chou, S. Y., Krauss, P. R., Renstrom, P. J., "Imprint of sub-25nm vias and trenches in polymers," Appl. Phys. Lett. 67, 3114-3116 (1995).
[2]   Chou, S. Y., Krauss, P. R., Renstrom, P. J., "Imprint lithography with 25-nanometer resolution," Science 272, 85-87 (1996).
[3]   Guo, L. J., "Recent progress in nanoimprint technology and its applications," J. Phys. D: Appl. Phys., 37, R123-R141 (2004).
[4]   Chou, S. Y., Krauss, P. R., "Imprint lithography with sub-10 nm feature size and high throughput," Microelect. Eng. 35, 237-240 (1997).
[5]   Austin, M. D., Ge, H., Wu, W., Li, M., Yu, Z., Wasserman, D., Lyon, S. A., Chou S. Y., "Fabrication of 5 nm linewidth and 14 nm pitch features by nanoimprint lithography," Appl. Phys. Lett. 84, 5299-5301 (2004).
[6]   F. Hua, Y. Sun, A. Guar, M. A. Meitl, L. Bilhaut, L. Rotkina, J. Wang, P. Geil, M. Shim, J. A. Rogers, "Polymer Imprint Lithography with Molecular-Scale Resolution," Nano Letters, 4, 2467 (2004).
[7]   Yan, X.-M., Kwon, S., Contreras, A. M., Bokor, J., Somorjai, G. A., "Fabrication of large number density platinum nanowire arrays by size reduction and nanoimprint lithography," Nano Letters 5, 745-748 (2005).
[8]   Park, S.-H., Lim, T.-W., Yang, D.-Y., Jeong, J.-H., Kim, K.-D., Lee, K.-S., Kong, H.-J., "Effective fabrication of three-dimensional nano/microstructures in a single step using multilayered stamp," Appl. Phys. Lett. 88, 203105 (2006).
[9]   Macintyre, D. S., Chen, Y., Lim, D., Thoms, S., "Fabrication of T gage structures by nanoimprint lithography," J. Vac. Sci. Technol. B, 19, 2797-2800 (2001).
[10]   Stewart, M. D., Willson C. G., "Imprint materials for nanoscale devices," MRS Bulletin, 30, 947-951 (2005).
[11]   Schmid, G. M., Stewart, M. D., Wetzel, J., Palmieri, F., Hao, J. Nishimura, Y., Jen, K., Kim, E. K., Resnick, D. J., Liddle, A., Wilson, C. G. "Implementation of an imprint damascene process for interconnect fabrication," J. Vac. Sci, Technol. B., 24, 1283-1291 (2006).

[12]   Matsui, S., Igaku, Y., Ishigaki, H, Fujita, J., Ishida, M., Ochiai, Y., Namatsu, H., Komuro, M., "Room-temperature nanoimprint and nanotransfer printing using hydrogen silsesquioxane," J. Vac. Sci. Technol. B, 21, 688-692 (2003).

[13]   Nakamatsu, K.-i., Watanabe, K., Tone, K., Katase, T., Hattori, W., Ochiai, Y., Matsuo, T., Sasago, M., Namatsu, H., Matsui, S., "Bilayer resist method for room-temperature nanoimprint lithography," Jap. J. Appl. Phys., 43, 4050-4053 (2004).

[14]   Chen, H. J. H., Liu, J. F., Hsu, Y. J., Syu, J. C. C., Huang, F. S., "Fabrication of Au nanowires on hydrogen silsequioxane by nanoimprint transfer," Nanotechnology, 16, 2913-2918 (2005).

[15]   Maex, K. Baklanov, M. R. Shamiryan, D. Lacopi, F. Brongersma, S. H. Yanovitskaya, Z. S., "Low dielectric constant materials for microelectronics," J. Appl. Phys., 93, 8793-8841(2003).

[16]   Morgen, M.; Ryan, E. T.; Zhao, J.-H.; Hu, C.; Cho, T.; and Ho, P. S., "Low dielectric constant materials for ULSI interconnects, Annu. Rev. Mater. Sci. 30, 645-680 (2000).

[17]   Miller, R. D. "In search of low-k dielectrics," Science 286, 421-423 (2001).

[18]   Cook, R. F., "Nanoporous glasses: Controlling crack propagation," Nature Materials, 3, 15-16 (2004).

[19]   Guyer, E. P., Dauskardt, R. H., "Fracture of nanoporous thin-film glasses," Nature Materials, 3, 53-57 (2004).

[20]   Maidenberg, D. A., Volksen, W., Miller, R. D., Dauskardt, "Toughning of Nanoporous Glasses using Porogen Residuals," Nature Materials, 3, 464-469 (2004).

[21]   Peters, L., "Making low-k dielectrics work," Semiconductor International, 29, 63-70 (2006).

[22]   H. J. Lee, C. L. Soles, D. W. Liu, B. J. Bauer, W. L. Wu, "Pore size distributions in low-k dielectric thin films from X-ray porosimetry," J. Polym. Sci., Part B: Polym. Phys. 40, 2170-2177 (2002).

[23]   H. J. Lee, C. L. Soles, D. W. Liu, B. J. Bauer, E. K. Lin, W. L. Wu, A. Grill, "Structural characterization of porous low- k thin films prepared by different techniques using x-ray porosimetry," J. Appl. Phys. 95, 2355-2359 (2004).

[24]   D. W. Gidley, W. E. Friez, T. L. Dull, J. Sun, A. F. Yee, C. V. Nguyen, and D. Y. Yoon, "Determination of Pore-Size Distribution in Thin Porous Films," Appl. Phys. Lett., 76, 1282-1284 (2000).

[25]   Dull, T. L., Frieze, W. E., Gidley, D. W., Sun, J. N., Yee, A. F., "Determination of pore size in mesoporous thin films from the annihilation lifetime of positronium," J. Phys. Chem. B, 105, 4657-4662 (2001).

[26]   H-G Peng, R. S. Vallery, M. Liu, W. E. Frieze,, J.-H. Yim, H-D. Jeong, J. Kim, and D. W. Gidley, "Deducing Pore Structure and Growth Mechanisms in Porogen-templated Silsesquioxane Thin Films," Appl. Phys. Lett., 87, 161903 (2005).

[27]   Lee, H.-J., Soles, C. L., Ro, H. W., Jones, R. L., Lin, E. K., Wu, W.-l., Heins, D. R., "Nanoimprint pattern transfer quality from specular x-ray reflectivity," Appl. Phys. Lett. 87, 263111 (2005).

[28]   H.-J. Lee, H.W. Ro, C.L. Soles, R.L. Jones, E.K. Lin, W. Wu, and D.R. Hines, "Effect of initial resist thickness on residual layer thickness of nanoimprinted structures," J. Vac. Sci. Tech. B, 23, 3023-3027 (2005).

[29]   Jones, R. L., Hu, T. J., Lin, E. K., Wu, W.-L., Kolb, R. K., Casa, D. M., Boulton, P., Barclay, G. G., " Small angle x-ray scattering for sub-100 nm pattern characterization," Appl. Phys. Lett. 83, 4059-4061 (2003).

[30]   Hu, T. J., Jones, R. L., Lin, E. K., Wu, W.-L., Keane, D., Weigand, S., Quintana, J. P., "Small angle x-ray scattering metrology for sidewall angle and cross section of nanometer scale line gratings," J. Appl. Phys. 96, 1983-1987 (2005).

[31]   Yoon, D. Y., Ro, H. W., Park, E. S., Lee, J.-K., Kim, H.-J., Char, K., Rhee, H.-W., Kwon, D., Gidley, D. W., "Structure and properties of polysilsesquioxanes and copolymers for ultra-low dielectric films," Mater. Res. Soc. Symp. Proc. 766, 241-251 (2003).

[32]   H. W. Ro, K. J. Kim, P. Theato, D. W. Gidley, D. Y. Yoon, "Novel inorganic-organic hybrid block copolymers as pore generators for nanoporous ultralow-dielectric-constant films," Macromolecules 38, 1031-1034 (2005).

[33]   Parratt, L. G., "Surface studies of solids by total reflection of X-rays, Phys. Rev. 95, 359-369 (1954).

[34]   Anker, J. F., Majkrzak, C. F., "Subsurface profile refinement for neutron specular reflectivity, in Neutron Optical Devices and Applications," SPIE Proceedings 1738; SPIE: Bellingham, WA, 1992, pg 260-268.

[35]   Hwang, S.-S., Lee, H.-C., Ro, H. W., Yoon, D. Y., Joo, Y.-C., "Effect of pore interconnection on Cu-diffuion-induced failures in porous spin-on low-k dielectrics," Appl. Phys. Lett. 87, 11915 (2005).

[36]   Chen, Z., Prasad, K., Jiang, N., Tang, L. J., Lu, P. W., Li, C. Y., "Silicon carbide based dielectric composites in bilayer sidewall barrier for Cu/porous ultralow-k interconnects," J. Vac. Sci, Technol. B 23, 1866-1872 (2005).

[37]   Hua, X., Kuo, M.-S., Oehrlein, G. S., Lazzeri, R., Iacob, E., Anderle, M., Inoki, C. K., Kuan, T. S., Jiang, P., Wu, W.-l., "Damage of ultralow k materials during photoresist mask stripping process," J. Vac. Sci. Technol. B. 24, 1238-1247 (2006).